PNAS RESEARCH ARTICLE | BIOPHYSICS AND COMPUTATIONAL BIOLOGY

Actin–microtubule dynamic composite forms responsive active matter with memory

Ondřej Kučera[a,1], Jérémie Gaillard[a], Christophe Guérin[a], Manuel Théry[a,b,1], and Laurent Blanchoin[a,b,1]

Edited by Yale Goldman, Pennsylvania Muscle Institute, University of Pennsylvania, Philadelphia, PA; received June 10, 2022; accepted June 21, 2022

Active cytoskeletal materials in vitro demonstrate self-organizing properties similar to those observed in their counterparts in cells. However, the search to emulate phenomena observed in living matter has fallen short of producing a cytoskeletal network that would be structurally stable yet possess adaptive plasticity. Here, we address this challenge by combining cytoskeletal polymers in a composite where self-assembling microtubules and actin filaments collectively self-organize due to the activity of microtubule-percolating molecular motors. We demonstrate that microtubules spatially organize actin filaments that in turn guide microtubules. The two networks align in an ordered fashion using this feedback loop. In this composite, actin filaments can act as structural memory and, depending on the concentration of the components, microtubules either write this memory or get guided by it. The system is sensitive to external stimuli, suggesting possible autoregulatory behavior in changing mechanochemical environments. We thus establish an artificial active actin–microtubule composite as a system demonstrating architectural stability and plasticity.

active materials | cytoskeleton | structural memory

Significance

Active cytoskeletal materials implemented up to now have been made mostly of chemically stabilized polymers and thus neglect the fundamental dynamical properties of living matter that confer its adaptability: growth, continuous renewal, and destructive remodeling. In this study, we overcome this limitation and develop a dynamic and active cytoskeletal composite based on assembling and disassembling filaments powered by molecular motors. In this system, we demonstrate the emergence of structural memory, which is an essential condition for the development of materials capable of learning or for understanding the mechanism, ensuring the consistency of intracellular organization despite its permanent renewing.

Active materials are composed of a large team of energy-dissipating constituents. Local interactions of these constituents lead to an emergence of a collective self-organizing behavior (1), which has been widely studied with networks of cytoskeleton filaments in vitro (2). From the transient formation of patterns like asters and vortices (3, 4) to constantly percolating active matter (5–9), which can be preprogrammed (10) or dynamically controlled (11), these synthetic out-of-equilibrium systems are considered to reconstitute, to a certain degree, the emergence of biological self-organization (2, 12). However, the ability of cells to develop, maintain, and adapt their internal organization is not a mere consequence of the reorganization of existing cellular components. Cells also dynamically assemble and disassemble their components. By this constant renewal of their cytoskeletal polymers, cells can maintain their architecture over longer periods, but they can also remodel it rapidly (13, 14). Since the active cytoskeletal networks implemented up to now have been made mostly of chemically stabilized polymers, they thus neglect fundamental dynamical properties that confer living matter with plasticity and adaptability.

Results

In the search to overcome this major limitation we wondered whether, in an in vitro assay, a combination of active self-organization of cytoskeletal polymers with their dissipative self-assembly could constitute a more realistic life-like matter. Inspired by recent research on cytoskeletal cross-talk (14, 15), we aimed at coalescing microtubules and actin filaments in a growing active composite. To do so, we developed a kinesin-driven motility assay of dynamic microtubules in the presence of growing actin filaments and a depletant. Unlike previously reported cytoskeletal composites, which relied on stabilized preassembled biopolymers (16, 17), our system includes the self-assembly in situ, enriching the set of possible behaviors.

First, we tested the behavior of each component separately. We attached kinesin-1 molecular motors to the passivated glass surface of the imaging chamber (Fig. 1*A*) and flowed in microtubule seeds that bind to the motors and glide in the presence of adenosine 5′-triphosphate (ATP). Free tubulin dimers added to the buffer together with guanosine triphosphate (GTP) enabled the elongation of microtubules from the seeds. A crowding agent included in the buffer (0.327% wt/vol 63-kDa methylcellulose) promoted cohesion of microtubules that are, otherwise, subject to electrostatic repulsion. In accordance with previous studies (9, 18), the resulting attraction manifests by the transient formation of microtubule bundles (Fig. 1*B*). These parallel and antiparallel bundles form as a result of the collisions of gliding microtubules (*SI Appendix*, Fig. S1).

Author affiliations: [a]CytoMorpho Lab, Laboratoire de Physiologie Cellulaire et Végétale, Interdisciplinary Research Institute of Grenoble, Commissariat à l'Énergie Atomique et aux Énergies Alternatives/CNRS/Université Grenoble Alpes, Grenoble, 38054 France; and [b]CytoMorpho Lab, Commissariat à l'Énergie Atomique et aux Énergies Alternatives/CNRS/Unité de Thérapie Cellulaire, Hôpital Saint Louis, Paris, 75010 France

Author contributions: O.K., M.T., and L.B. designed research; O.K. and J.G. performed research; J.G. and C.G. contributed new reagents/analytic tools; O.K. analyzed data; and O.K., M.T., and L.B. wrote the paper.

The authors declare no competing interest.

This article is a PNAS Direct Submission.

[1]To whom correspondence may be addressed. Email: ondrej.kucera@biophysics.cz, manuel.thery@cea.fr, or laurent.blanchoin@cea.fr.

This article contains supporting information online at http://www.pnas.org/lookup/suppl/doi:10.1073/pnas.2209522119/-/DCSupplemental.

Published July 25, 2022.

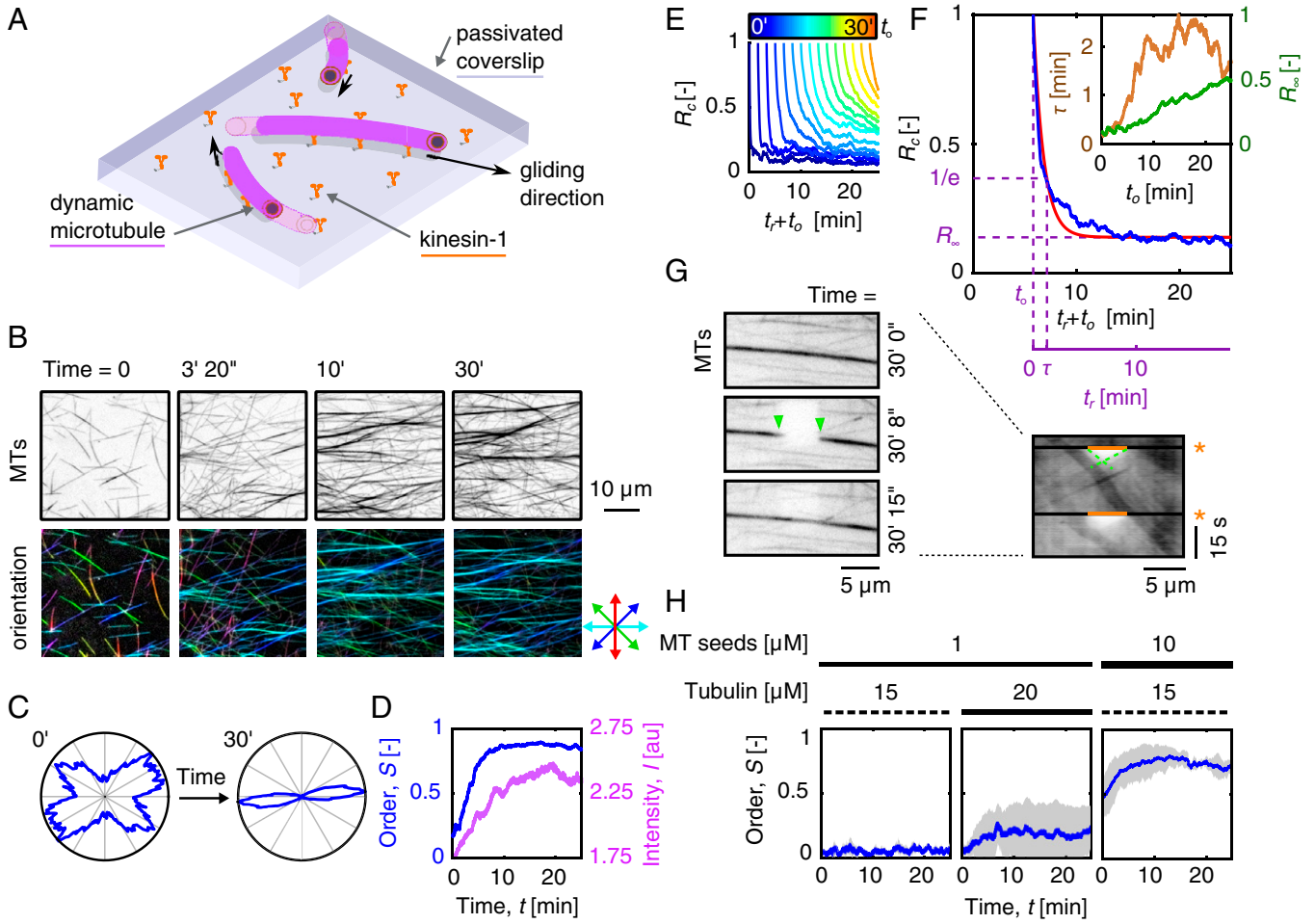

Fig. 1. Motile dynamic microtubule system self-organizes into quasi-parallel microtubule streams. (*A*) Schematic representation of the system. (*B*) Intensity inverted fluorescence micrographs of dynamic microtubule motility assay (*Top*) and the corresponding color-coded orientation analysis (*Bottom*). (*C*) Polar histogram of the orientation of microtubules is narrowing with time. (*D*) Time trace of the global order, *S*, and fluorescence intensity, *I*, of dynamic microtubules in the motility assay. (*E*) Time traces of equidistant vertical slices of Pearson correlation coefficient matrix of fluorescence micrographs of dynamic microtubule motility assay. (*F*) The correlation slices in *E* can be approximated by an exponential decay with the parameters of the correlation decay time (time constant) and asymptotic correlation amplitude and represented by corresponding temporal profiles (*Inset*). (*G*) Intensity inverted fluorescence micrographs of photobleaching of microtubule stream (*Left*; green arrowheads indicate the limits of photobleached area) formed during 30 min of ordering and the corresponding kymograph (*Right*; orange lines indicate the photobleached area, green dashed lines indicate the front of receding photobleached areas, and asterisks denote the time of photobleaching). (*H*) Time traces of the global order for various initial concentrations of microtubule seeds and free tubulin. All experiments were repeated at least four times with similar results. Data in *H* are represented as mean value (solid blue line) ± SD (shaded area) ($n = 4$ per condition).

The growth of microtubules translates into increased surface occupancy and increases the probability of their collisions. Consequently, the initially short, disordered microtubules evolve in an ordered network of long, quasi-aligned microtubule streams (Fig. 1*B* and *C*, *SI Appendix*, Fig. S2, and Movie S1), and so the global nematic order, a metric of orientation ordering, grows until it saturates, preceding the saturation of microtubule assembly (Fig. 1*D* and *SI Appendix*, Fig. S3). Correlation analysis revealed that these streams form increasingly stable architecture (Fig. 1*E* and *F* and *SI Appendix*, Fig. S4) despite being supported by dynamic microtubules that stay motile within the streams, as photobleaching experiments confirmed (Fig. 1*G* and Movie S2). The dynamic instability of microtubules could be seen at the initial stage of the experiments (*SI Appendix*, Fig. S5), but as the microtubules grew and aligned we neither observed behavior that could be undoubtedly interpreted as dynamic instability nor could we distinguish such behavior from the population of microtubule tip velocities (*SI Appendix*, Fig. S6). Notably, the concentration of free tubulin and microtubule seeds in the assay has to exceed a certain threshold for the emergence of such stable orientation order (Fig. 1*H*); the microtubule seeds do not self-organize in the absence of free tubulin (*SI Appendix*, Fig. S7). The estimation of the average microtubule length, 25 µm (10 µM seeds, 15 µM free tubulin), 64 µm (1 µM seeds, 15 µM free tubulin), and 88 µm (1 µM seeds, 20 µM free tubulin), showed trends consistent with microtubule elongation kinetics: Decreasing the concentration of nucleation centers leads to longer microtubules, and increasing the concentration of tubulin increases the length further. The density of microtubules, their elongation, and thus the probability of their collisions, are, therefore, central to the self-organizing behavior we observed.

Next, we studied the ordering of growing actin filaments in the experimental chamber in the absence of microtubules (Fig. 2*A* and Movie S3). Actin filaments are not motile in our assay since they do not interact with kinesin motors. Crowding agent (methylcellulose) depletes actin filaments from the volume of the chamber to the glass surface, where a growing network forms locally nematic order (Fig. 2*B*), similar to a previous report (19). As a result, in contrast to motile microtubules, the actin network alone does not show orientationally ordered architecture at a larger scale (Fig. 2*C* and *D* and *SI Appendix*, Fig. S8). Importantly, as the increasing surface occupancy reduces the mobility

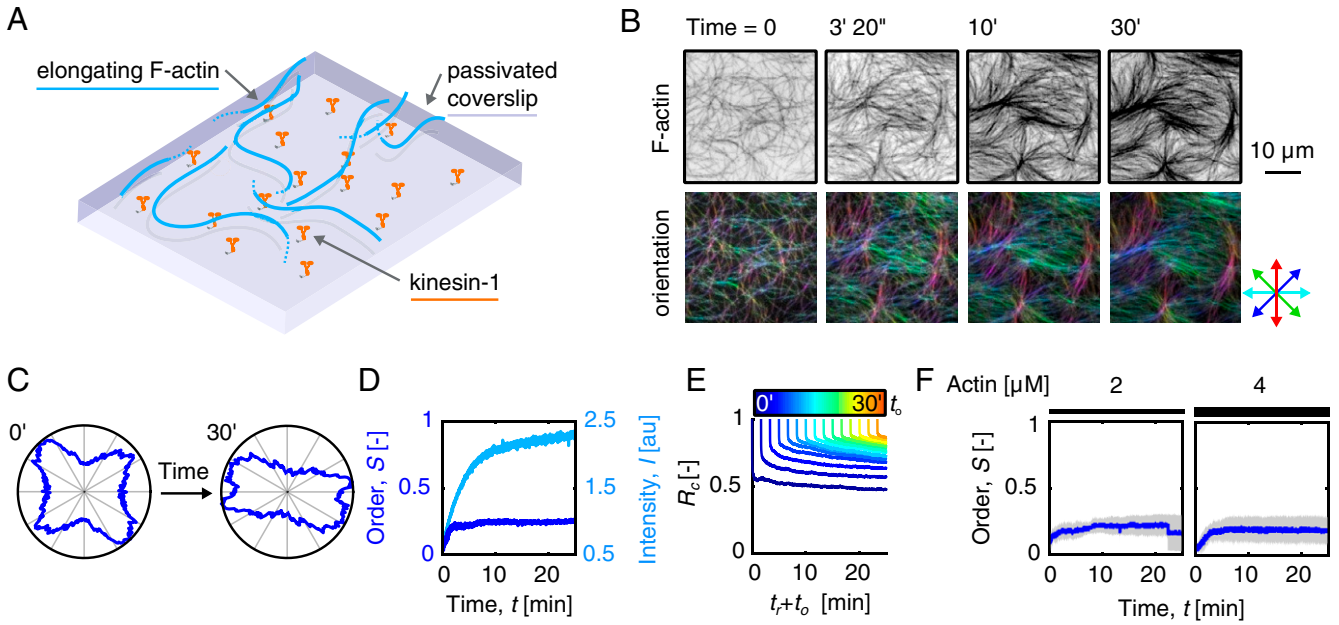

Fig. 2. Assembling actin filaments self-organize in a locally nematic fashion with low global order. (*A*) Schematic representation of the system. (*B*) Intensity inverted fluorescence micrographs of dense elongating actin filaments (*Top*) and the corresponding color-coded orientation analysis (*Bottom*) show local nematic ordering. (*C*) Polar histogram of the orientation of actin filaments is narrowing only a little with time, indicating low global order. (*D*) Time trace of the global order, *S*, and fluorescence intensity, *I*, of growing actin system. (*E*) Time traces of equidistant vertical slices of Pearson correlation coefficient matrix of fluorescence micrographs of growing actin system. (*F*) Time traces of the global order for two initial concentrations of free actin monomers. All experiments were repeated at least four times with similar results. Data in *F* are represented as mean value (solid blue line) ± SD (shaded area) (n = 4 per condition).

of the filaments their organization remains structurally stable, as the correlation analysis showed (Fig. 2*E*). A photobleaching experiment further confirmed that there is no substantial turnover of actin within the observation timeframe (*SI Appendix*, Fig. S9). Varying the concentration of actin monomers within the range used in this study did not affect this emerging organization significantly (Fig. 2*F*).

After demonstrating that motile dynamic microtubules form self-renewing ordered architecture while growing actin forms a stable network, we merged these polymers in a composite system (Fig. 3*A*) and studied how the interactions between them influence the ordering behavior. Our central observation is that they do interact with each other. When microtubules encountered actin filaments, they occasionally caught the filaments and moved them temporarily, effectively organizing the actin network (Fig. 3*B* and Movie S4). More often, though, microtubules and actin filaments interacted cohesively. In such a case, denser regions of the actin network steered the microtubule trajectory, effectively guiding gliding microtubules (Fig. 3*C* and Movie S5). These mutual interactions combine and constitute a feedback loop where microtubules organize actin filaments that in turn guide microtubules (Fig. 3*D*). Within a few minutes after starting the experiment, this feedback in the dynamic composite system gave rise to an alignment between microtubules and actin filaments, which are forming overlapping streams and bundles, respectively (Fig. 3*E* and Movie S6). The reaching of this steady order preceded the saturation of the assembly of both cytoskeletal components (Fig. 3*F*). The upper limit of actin reorganization estimated from the lag between the actin ordering and the polymerization curve is reaching 50% of the final mass of the polymerized actin. In the composite, the estimated average microtubule length rose from 88 µm to 194 µm, providing a solid indication that actin filaments stabilized the microtubules. By comparing the structural stability of the composite with that of microtubules alone, we concluded that actin also stabilizes the emerging order (compare *SI Appendix*, Figs. S3, S4, S8, and S10). An unexpected manifestation of this behavior is that we could consistently observe the ordering of microtubules at a density that would not support ordering in the absence of an actin network (Fig. 3*G* and *SI Appendix*, Fig. S3).

To further investigate this unexpected emerging property of the composite, we tested how it would respond to the removal of one of its components. When we depolymerized microtubules either by adding $CaCl_2$ or decreasing the temperature below 12 °C, the actin network retained its ordering thanks to its cohesion and low turnover (Fig. 4*A* and Movie S7). Strikingly, when we, instead of microtubules, disassembled actin filaments using gelsolin, an actin-severing protein, we observed microtubule dispersion (Fig. 4*B* and Movie S8). These observations highlight the role of the actin network in maintaining the order of microtubules over time.

Importantly, these data suggest that actin acts as long-term structural memory for the microtubule network. We tested this hypothesis by reassembling microtubules after their depolymerization. First, we let microtubules self-organize into streams in the absence of actin. After temperature-dependent depolymerization, we repolymerized the microtubules by increasing the temperature in the chamber. We observed that microtubules self-organized in streams again, but, importantly, the orientation of the streams was random and different from the initial orientation before the temperature shift (Fig. 4*C* and Movie S9). However, when we repeated this cycle in the presence of actin filaments, we witnessed a striking behavior: The newly polymerized microtubule network recovered the ordering and orientation it had before disassembly (Fig. 4*D* and Movie S10). Therefore, microtubules could sense the order that was conserved in the organization of the actin network, which does not undergo substantial remodeling even on the local scale (*SI Appendix*, Fig. S11). Actin filaments in our composite thus form a structural memory that acts as a template to sustain microtubule organization (Fig. 4*E*) (20, 21).

To test whether microtubules could also sense the order implied on the actin by an external factor, we organized

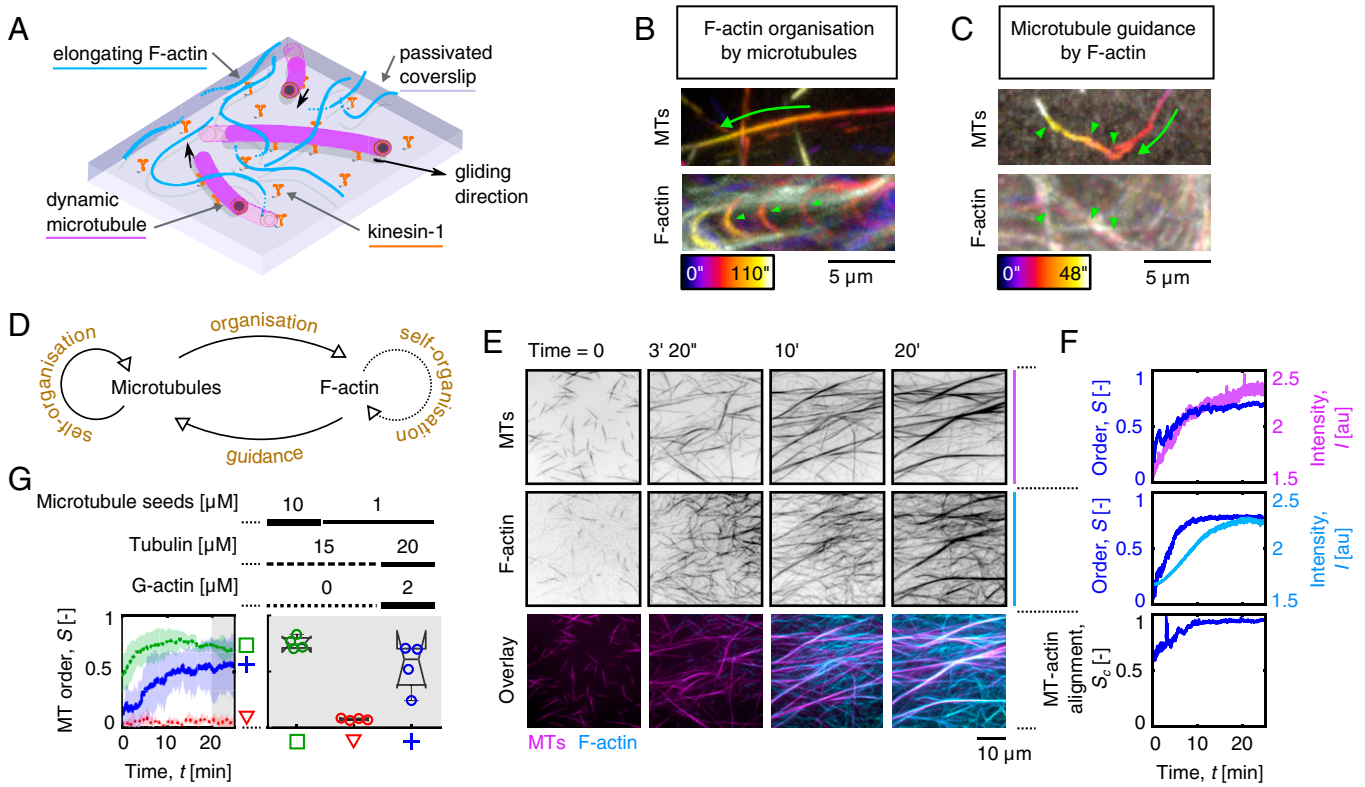

Fig. 3. Interactions between microtubules and actin filaments mutually promote the self-organization of the cytoskeletal composite. (*A*) Schematic representation of the system. (*B*) Color-coded maximum fluorescence intensity projections of gliding microtubule (*Top*) pushing actin filaments (*Bottom*), effectively organizing them. (*C*) Gliding microtubule steered and guided by actin filaments. Image representation as in *B*. (*D*) Schematic representation of the interactions forming a feedback loop between actin and microtubules. (*E*) Multichannel fluorescence micrographs of self-assembling and self-organizing actin-microtubule composite. Individual fluorescence channels are displayed as intensity inverted images. The overlay image is noninverted for clarity. (*F*) Time traces of the global order, *S*, and fluorescence intensity, *I*, of microtubules (*Top*) and actin filaments (*Center*), and their mutual alignment, S_c, (*Bottom*) in the composite system. (*G*) Time traces of the global order of microtubules (*Left*) and the corresponding steady-state order (*Right*) for three indicated initial biochemical conditions. All experiments were repeated at least four times with similar results. Data in *G* are represented as mean value ± SD (*Left*) and median ± 75th percentile (*Right*), where notches display the variability of the median between samples ($n = 4$ per condition).

phalloidin-stabilized actin filaments in semiparallel bundles using hydrodynamic preordering (*SI Appendix*, Fig. S12), which resulted in a stable order (*SI Appendix*, Fig. S13). Microtubules were guided by this organization and aligned with actin filaments (*SI Appendix*, Fig. S12), similarly to previous experiments. Nevertheless, we note that the feedback loop between actin guidance and microtubule organization (Fig. 3*D*) has limits, documented by the inability of microtubules to align with or reorganize stabilized and randomly preordered actin mesh (*SI Appendix*, Fig. S12). The coassembly and mutual self-organization of actin filaments and microtubules in our composite overcome this limitation.

Discussion

The ability of the polymerized and ordered actin network to impose its order on microtubules reflects its structural stability. The stability stems from the low intrinsic actin turnover (22) and entropic cohesion due to the presence of methylcellulose, a crowding agent (23–25), which practically limits the possibility of network remodeling. This is in sharp contrast with the initial phase of the composite self-assembly when the ordering and alignment of biopolymers occur. At this stage of lower surface polymer density, growing and gliding microtubules organize actin filaments into a steady conformation that will, in turn, guide microtubules. This feedback loop, together with the continuation of the polymerization, reinforces the spatial ordering of the composite, highlighting the importance of the self-assembling nature of the composite for its emerging properties. Notably, the order that is supported by the actin memory in our system is reversible as it can be annihilated by chemical signaling in the presence of regulatory proteins. Fine-tuning of the actin or microtubule turnover, which is intrinsic to biological systems, might thus constitute a means of precise tuning of the emergent order.

The observed low turnover of actin filaments corresponds to the expected k_{off} of actin filaments at their pointed ends of approximately 0.27 s^{-1} under the conditions of our study (26). The indication that actin filaments stabilized the microtubules is consistent with a previous report (27). This additional emerging property of our composite may contribute to the reinforcement of the order in our system. Even though the protein turnover is low in our system, the use of nonstabilized self-assembling cytoskeletal polymers is instrumental to the observed behavior. First, it is a prerequisite for reversible microtubule destruction and the demonstration of the memory effect. Second, the growth of microtubules increases the probability of microtubule collisions and subsequent alignment. At initial lengths and densities, the microtubules do not self-organize, which is consistent with previously published results (17). On the side of actin, the assembly is essential to the alignment with microtubules since only less than 50% of actin filaments are subject to reorganization by microtubules. Experiments with stabilized actin structures confirmed that microtubules were not able to reorganize stabilized actin efficiently. Microtubules were able to align with stabilized actin filaments that had semiparallel order. However, microtubules could not efficiently read the disordered random actin structure,

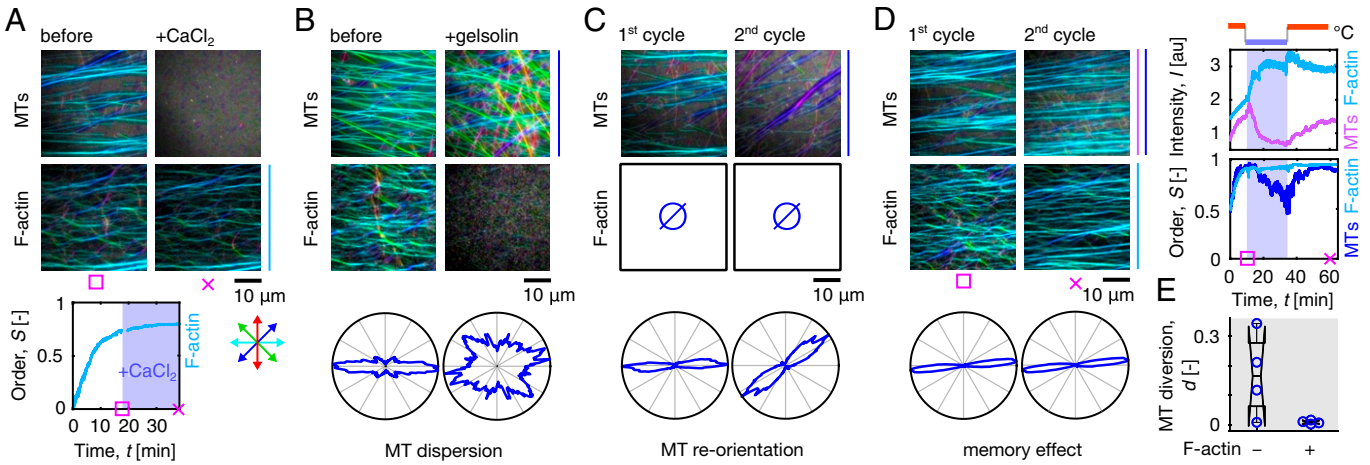

Fig. 4. Response of the cytoskeletal composite to chemical and physical perturbations reveal the structural memory of the system. (*A*) Color-coded orientation analysis of microtubules (*Top*) and actin filaments (*Center*) before (*Left*) and after (*Right*) the addition of $CaCl_2$. Corresponding time trace of the global actin order (*Bottom*). (*B*) Orientation color-coded maximum fluorescence intensity projection (200 s) of microtubules (*Top*) and orientation color-coded micrographs of actin filaments before (*Left*) and after (*Right*) the addition of gelsolin. Corresponding polar histograms of microtubule orientation (*Bottom*) show microtubule dispersion. (*C*) Color-coded orientation analysis of microtubules (*Top*) after the first (*Left*) and second (*Right*) cycle of microtubule polymerization in the absence of actin. Corresponding polar histograms of microtubule orientation (*Bottom*) show reorientation in different directions. (*D*) Color-coded orientation analysis of microtubules (*Top*) and actin filaments (*Center*) after the first (*Left*) and second (*Right*) cycle of microtubule polymerization. Corresponding polar histograms of microtubule orientation (*Bottom*) show the retention of the orientation. Time traces of the fluorescence intensities (*Top Right*) and global order (*Bottom Right*) of microtubules and actin filaments. The shaded area corresponds to the cooling cycle. (*E*) Diversion of repolymerized microtubules (second cycle) from the dominant direction before depolymerization (first cycle) in the absence and presence of F-actin memory as in examples shown in *C* and *D*, respectively.

likely due to the mismatch between the persistence length of microtubules and the waviness of the actin network, which prevented efficient guidance. We note that stabilized actin filaments always created a clear bundled structure, a feature related to the prepolymerization at high actin concentrations before dilution in the imaging buffer. This is in sharp contrast with actin filaments polymerized in situ (Fig. 2), which maximize their surface occupancy similarly to dense nonmotile microtubules in the presence of a crowding agent (28, 29). It is possible that this bundled structure further prevented the reorganization by microtubules.

In a cell, the timescales of cytoskeletal remodeling, and many other cytoskeleton-related phenomena, may not quantitatively match the in vitro observations. We may expect that the physical guidance of the templated growth in cells would be more complex than in our observations, where the cohesion is nonspecific due to the action of the depletant. The landscape of interactions would not be limited to entropic forces in a cellular context. It would include specific cross-linkers of both passive and active character and a plethora of regulatory factors. Despite these differences and a possible quantitative mismatch of the dynamics, our system manifests several basic principles of templating and remodeling and emerging structural memory of the cytoskeleton that has been described during cellular self-organization of the cytoskeleton. First, cytoskeletal filaments can support self-templated growth, for example during filament-guided filament assembly of the actin network in *Caenorhabditis elegans* embryos (21). Second, one cytoskeletal network can serve as a template for the growth of another network, such as during microtubule guidance alongside actin bundles in growing neuronal tips (30, 31), or along intermediate filaments (20). Although these two mechanisms likely combine, the latter can support a higher diversity of outcomes due to the combination of two populations of filaments with different lifetimes, specificity for regulatory factors, and mechanical properties. The system we present here combines both types of structural templating observed in living matter but reserves the long-term memory for actin filaments, emphasizing its composite character.

Introducing dissipative self-assembly of the constituting filaments to an active cytoskeletal composite is, therefore, critical for the emergence of adaptive architecture with concurrent plasticity and stability. While this feature is highly relevant for biological questions, it may also serve as a basis for developing diverse artificial systems, including life-like materials (32, 33) and synthetic cells (34, 35).

Materials and Methods

Protein Production and Purification. Actin and tubulin were purified and labeled as described previously (36). Briefly, bovine brain tubulin was isolated in temperature-dependent cycles of polymerization and depolymerization (37) and purified from associated proteins (microtubule-associated proteins) by cation exchange chromatography. Soluble tubulin was stored in the BRB80 buffer (80 mM Pipes, pH 6.8, 1 mM EGTA, and 1 mM $MgCl_2$) in liquid nitrogen. Rabbit skeletal muscle actin was purified from acetone powder (38). The actin was gel-filtered and stored in G-buffer (2 mM Tris·HCl, pH 8.0, 0.2 mM ATP, 0.5 mM dithiothreitol [DTT], 0.1 mM $CaCl_2$, and 0.01% sodium azide) at 4 °C. Parts of the tubulin and actin were labeled with Atto 488 and Alexa 568 fluorophores (Molecular Probes), respectively, by NHS ester coupling (39) and stored as the unlabeled proteins. All experiments were carried out with 20% labeled tubulin and 5% labeled actin. Microtubule seeds were polymerized in the presence of GMPCPP. Recombinant, truncated kinesin-1-GFP (green fluorescent protein) motor and gelsolin were expressed in *Escherichia coli* cells and purified similarly to previously reported methods (40, 41) and stored at −80 °C.

In Vitro Assay. The in vitro gliding assay was performed in a flow chamber of approximately 15 µL, which was assembled from NaOH-cleaned glass coverslips using double-sided tape as a spacer. The channel's surface was functionalized by GFP polyclonal antibodies (Invitrogen, A-11122) by filling the channel with 100 $\mu g \cdot mL^{-1}$ antibodies in HKEM buffer (10 mM Hepes, pH 7.2, 5 mM $MgCl_2$, 1 mM EGTA, and 50 mM KCl) for 3 min. The remaining available surface was then passivated by introducing 1% wt/vol bovine serum albumin (BSA) in HKEM buffer for 5 min. Next, kinesin-1-GFP motors (60 $\mu g \cdot mL^{-1}$ in wash buffer: 10 mM Hepes, pH 7.2, 16 mM Pipes buffer, pH 6.8, 50 mM KCl, 5 mM $MgCl_2$, 1 mM EGTA, 20 mM DTT, 3 $mg \cdot mL^{-1}$ glucose, 20 $\mu g \cdot mL^{-1}$ catalase, 100 $\mu g \cdot mL^{-1}$ glucose oxidase, and 0.3% wt/vol BSA) were specifically attached to the antibodies during 3 min of incubation. The channel was then perfused

with wash buffer, and microtubule seeds (average length 4.07 ± 1.53 μm, 10 μM or 1 μM polymerized tubulin in wash buffer) were optionally introduced for 5 min of incubation, during which the seeds attached to kinesin motors. The unbound microtubules were washed away with wash buffer. The resulting surface density of microtubule seeds was 0.12 μm^{-2} and 0.016 μm^{-2} for 10 μM and 1 μM seeds, respectively. Finally, the imaging Tic-Tac buffer (10 mM Hepes, pH 7.2, 16 mM Pipes, pH 6.8, 50 mM KCl, 5 mM $MgCl_2$, 1 mM EGTA, 20 mM DTT, 3 mg·mL^{-1} glucose, 20 μg·mL^{-1} catalase, 100 μg·mL^{-1} glucose oxidase, 2.67 mM ATP, 1 mM GTP, 0.3% wt/vol BSA, and 0.327% wt/vol methylcellulose [63 kDa, Sigma-Aldrich, M0387]) was introduced. Free tubulin (20% labeled and 80% unlabeled tubulin) and actin (12% labeled and 88% unlabeled actin) were added to the imaging Tic-Tac buffer optionally, with concentrations indicated in the main text. The flow chamber was optionally sealed by a capillary tube sealant (Vitrex) and transferred for imaging.

In the experiment with chemical actin and microtubule disassembly, the channel was kept open, and the environment was humidified to prevent evaporation. To induce actin disassembly, a 2-μL drop of 80 μM gelsolin and 10 μM tubulin mixture (to prevent microtubule depolymerization) in the imaging Tic-Tac buffer was dripped to the channel opening. The proteins reached the imaging area by diffusion. To prevent flow-induced reorganization of the cytoskeletal networks, no additional flow was used. After equilibration, the concentration of gelsolin was ∼10 μM. To depolymerize microtubules chemically, ∼10 μM final concentration $CaCl_2$ was used. To depolymerize microtubules by a physical factor, the temperature was decreased to ∽12 °C. Microtubules were repolymerized by increasing the temperature to 37 °C again.

Control experiments were performed using stabilized actin filaments assembled in the presence of 1 μM phalloidin before the start of the experiment. A flow chamber with the applied flow or flowless imaging well were used to create actin semiparallel or random actin organization, respectively.

Imaging. Microtubules and actin filaments were imaged by total internal reflection fluorescence microscopy using an inverted microscope (Eclipse Ti, Nikon) with 100× 1.49 numerical aperture oil-immersion objective (UApo N, Olympus). The Atto 488 and Alexa 568 fluorophores were excited by 491-nm and 561-nm lasers (Optical Insights), respectively, through the $iLas^2$ dual laser illuminator (Roper Scientific). The fluorescence signals were separated by the Dual-View beam splitter (Optical Insights) and recorded by the Evolve 512 EMCCD camera (Photometrics). The sample was mounted to the environmental chamber maintained at 37 °C and, optionally, at high relative humidity. To cool the sample down to depolymerize microtubules, the heating was turned off. The accumulated heat was transferred to a precooled bath, leading to a temperature of ∽12 °C measured by a sensor attached to the microscope objective. The photobleaching of microtubule streams was performed using an ultraviolet (UV) laser at the end of the experiments. The photobleaching of actin was performed after the saturation of the fluorescence growth curve using a UV laser, The imaging was controlled by Metamorph software (v. 7.7.5, Universal Imaging), with images taken every second.

Image Processing and Data Analysis. Images were processed by Fiji (v 1.52) (42) and custom MATLAB (v 9.6, MathWorks, Inc.) procedures using the MIJ (43) for running Fiji within MATLAB. For presentation purposes, the contrast of images was adjusted. For analysis, the background of the 488 channel was subtracted using the built-in ImageJ function. The temporal profiles of the mean fluorescence intensities were obtained from ImageJ Plot *z* axis function. The kymographs were generated using the Multikymograph ImageJ plugin. As a measure of the orientation, we used the nematic ordering parameter, *S*, estimated from the mean resultant length of the director field (44). The value of *S* was calculated in MATLAB from the weighted histogram of the orientation director field, which was obtained by OrientationJ plugin (45, 46), as

$$S(t) = \frac{1}{\sum_{\phi\in\left[-\frac{\pi}{2},\frac{\pi}{2}\right]} N(t,\phi)} \sqrt{\left(\sum_{\phi\in\left[-\frac{\pi}{2},\frac{\pi}{2}\right]} N(t,\phi)\cos(2\phi)\right)^2 + \left(\sum_{\phi\in\left[-\frac{\pi}{2},\frac{\pi}{2}\right]} N(t,\phi)\sin(2\phi)\right)^2},$$

where $N(t,\phi)$ is the number of pixels oriented in the direction of angle ϕ at time t with coherency higher than 10%. The local angular difference was measured as a difference between the dominant orientation of the director field within a sliding window of the size of 5.76 μm^2 at the indicated times of the observation.

The mutual ordering parameter was calculated from the orientation director, O_{MT} and O_a, and the orientation energy, E_{MT} and E_a, fields, which were obtained by the OrientationJ plugin, as

$$S_c(t) = \frac{1}{N^2}\sum_{i=1}^{N}\sum_{j=1}^{N}\left(\cos\left(M_{(i,j)}(t)\left(O_{MT(i,j)}(t) - O_{a(i,j)}(t)\right)\right)\right)^2,$$

where (i,j) denotes the index within an image and the mask, *M*, is defined as

$$M_{(i,j)}(t) = 1 \ \ldots\ E_{MT(i,j)}(t) > 0.05 \ \wedge\ E_{a(i,j)}(t) > 0.05$$
$$M_{(i,j)}(t) = 0 \ \ldots\ \text{otherwise}.$$

To quantify the stability of the network organization, the Pearson correlation coefficient of each frame of the experiment with all the consecutive frames was calculated. An exponential decay can approximate each series with two parameters: the correlation decay time (time constant), τ, and the asymptotic correlation amplitude. The correlation coefficients and curve fitting were calculated using built-in MATLAB functions.

Average microtubule lengths were estimated by extrapolating the initial length of microtubules using the increase of the background-subtracted microtubule fluorescence intensity. Microtubule tip velocities were measured manually from kymographs of the microtubule streams after the saturation of microtubule growth.

The diversion of dominant orientation of repolymerized microtubules (second cycle), ϕ_2, from the orientation before the depolymerization (first cycle), ϕ_1, was calculated as $d = 1 - \cos(\phi_1 - \phi_2)$.

Graphs were produced using MATLAB, and the final figures were formatted using Inkscape. At least three independent experiments were performed for each condition if not stated otherwise. No data were excluded from the study.

Data Availability. All study data are included in the article and/or supporting information. The microscopic image series are available from the corresponding author upon reasonable request.

ACKNOWLEDGMENTS. We thank Magali Orhant-Prioux, Alexandre Schaeffer, and Guillaume Schiano-Lomoriello for technical support. This work was supported by European Research Council Consolidator Grant 771599 (ICEBERG) to M.T. and Advanced Grant 741773 (AAA) to L.B. O.K. was partially supported by Pôle emploi (7820342X). Our imaging platform is supported by the Laboratory of Excellence Grenoble Alliance for Integrated Structural & Cell Biology (LabEX GRAL) (ANR-10-LABX-49-01) and the University Grenoble Alpes graduate school (Ecoles Universitaires de Recherche) (CBH-EUR-GS, ANR-17-EURE-0003).

1. M. R. Shaebani, A. Wysocki, R. G. Winkler, G. Gompper, H. Rieger, Computational models for active matter. *Nat. Rev. Phys.* **2**, 181–199 (2020).
2. D. Needleman, Z. Dogic, Active matter at the interface between materials science and cell biology. *Nat. Rev. Mater.* **2**, 10.1038/natrevmats.2017.48. (2017).
3. F. J. Nédélec, T. Surrey, A. C. Maggs, S. Leibler, Self-organization of microtubules and motors. *Nature* **389**, 305–308 (1997).
4. T. Surrey, F. Nédélec, S. Leibler, E. Karsenti, Physical properties determining self-organization of motors and microtubules. *Science (80-.)* **292**, 1167–1171 (2001).
5. T. Sanchez, D. T. N. Chen, S. J. DeCamp, M. Heymann, Z. Dogic, Spontaneous motion in hierarchically assembled active matter. *Nature* **491**, 431–434 (2012).
6. G. Duclos *et al.*, Topological structure and dynamics of three-dimensional active nematics. *Science (80-.)* **1124**, 1120–1124 (2020).
7. Y. Sumino *et al.*, Large-scale vortex lattice emerging from collectively moving microtubules. *Nature* **483**, 448–452 (2012).
8. A. Sciortino, A. R. Bausch, Pattern formation and polarity sorting of driven actin filaments on lipid membranes. *Proc. Natl. Acad. Sci. U.S.A.* **118**, 1–8 (2021).
9. D. Inoue *et al.*, Depletion force induced collective motion of microtubules driven by kinesin. *Nanoscale* **7**, 18054–18061 (2015).
10. A. J. M. Wollman, C. Sanchez-Cano, H. M. J. Carstairs, R. A. Cross, A. J. Turberfield, Transport and self-organization across different length scales powered by motor proteins and programmed by DNA. *Nat. Nanotechnol.* **9**, 44–47 (2014).
11. T. D. Ross *et al.*, Controlling organization and forces in active matter through optically defined boundaries. *Nature* **572**, 224–229 (2019).
12. T. Vignaud, L. Blanchoin, M. Théry, Directed cytoskeleton self-organization. *Trends Cell Biol.* **22**, 671–682 (2012).
13. T. Misteli, The concept of self-organization in cellular architecture. *J. Cell Biol.* **155**, 181–185 (2001).
14. M. Dogterom, G. H. Koenderink, Actin–microtubule crosstalk in cell biology. *Nat. Rev. Mol. Cell Biol.* **20**, 38–54 (2018).

15. F. Huber, A. Boire, M. P. López, G. H. Koenderink, Cytoskeletal crosstalk: When three different personalities team up. *Curr. Opin. Cell Biol.* **32**, 39–47 (2015).
16. G. Lee *et al.*, Myosin-driven actin-microtubule networks exhibit self-organized contractile dynamics. *Sci. Adv.* **7**, 1–10 (2021).
17. L. Farhadi, C. Fermino Do Rosario, E. P. Debold, A. Baskaran, J. L. Ross, Active self-organization of actin-microtubule composite self-propelled rods. *Front. Phys.* **6**, 1–16 (2018).
18. A. Saito *et al.*, Understanding the emergence of collective motion of microtubules driven by kinesins: Role of concentration of microtubules and depletion force. *RSC Advances* **7**, 13191–13197 (2017).
19. D. S. Seara *et al.*, Entropy production rate is maximized in non-contractile actomyosin. *Nat. Commun.* **9**, 4948 (2018).
20. Z. Gan *et al.*, Vimentin intermediate filaments template microtubule networks to enhance persistence in cell polarity and directed migration. *Cell Syst.* **3**, 252–263.e8 (2016).
21. Y. Li, E. Munro, Filament-guided filament assembly provides structural memory of filament alignment during cytokinesis. *Dev. Cell* **56**, 2486–2500.e6 (2021).
22. L. Blanchoin, R. Boujemaa-Paterski, C. Sykes, J. Plastino, Actin dynamics, architecture, and mechanics in cell motility. *Physiol. Rev.* **94**, 235–263 (2014).
23. A. Ward *et al.*, Solid friction between soft filaments. *Nat. Mater.* **14**, 583–588 (2015).
24. F. Hilitski *et al.*, Measuring cohesion between macromolecular filaments one pair at a time: Depletion-induced microtubule bundling. *Phys. Rev. Lett.* **114**, 138102 (2015).
25. M. Braun, Z. Lansky, F. Hilitski, Z. Dogic, S. Diez, Entropic forces drive contraction of cytoskeletal networks. *BioEssays* **38**, 474–481 (2016).
26. T. D. Pollard, Rate constants for the reactions of ATP- and ADP-actin with the ends of actin filaments. *J. Cell Biol.* **103**, 2747–2754 (1986).
27. A. Colin, P. Singaravelu, M. Théry, L. Blanchoin, Z. Gueroui, Actin-network architecture regulates microtubule dynamics. *Curr. Biol.* **28**, 2647–2656.e4 (2018).
28. B. Edozie *et al.*, Self-organization of spindle-like microtubule structures. *Soft Matter* **15**, 4797–4807 (2019).
29. S. Sahu, L. Herbst, R. Quinn, J. L. Ross, Crowder and surface effects on self-organization of microtubules. *Phys. Rev. E* **103**, 062408 (2021).
30. S. Biswas, K. Kalil, The microtubule-associated protein tau mediates the organization of microtubules and their dynamic exploration of actin-rich lamellipodia and filopodia of cortical growth cones. *J. Neurosci.* **38**, 291–307 (2018).
31. C. Sánchez-Huertas *et al.*, The +TIP Navigator-1 is an actin-microtubule crosslinker that regulates axonal growth cone motility. *J. Cell Biol.* **219**, e201905199 (2020).
32. A. Walther, Viewpoint: From responsive to adaptive and interactive materials and materials systems: A roadmap. *Adv. Mater.* **32**, e1905111 (2020).
33. C. Kaspar, B. J. Ravoo, W. G. van der Wiel, S. V. Wegner, W. H. P. Pernice, The rise of intelligent matter. *Nature* **594**, 345–355 (2021).
34. Y. Elani, Interfacing living and synthetic cells as an emerging frontier in synthetic biology. *Angew. Chem. Int. Ed.* **60**, 5602–5611 (2020).
35. P. Schwille *et al.*, MaxSynBio: Avenues towards creating cells from the bottom up. *Angew. Chem. Int. Ed. Engl.* **57**, 13382–13392 (2018).
36. M. Vantard, C. Peter, A. Fellous, P. Schellenbaum, A. M. Lambert, Characterization of a 100-kDa heat-stable microtubule-associated protein from higher plants. *Eur. J. Biochem.* **220**, 847–853 (1994).
37. M. L. Shelanski, Chemistry of the filaments and tubules of brain. *J. Histochem. Cytochem.* **21**, 529–539 (1973).
38. J. A. Spudich, S. Watt, The regulation of rabbit skeletal muscle contraction. I. Biochemical studies of the interaction of the tropomyosin-troponin complex with actin and the proteolytic fragments of myosin. *J. Biol. Chem.* **246**, 4866–4871 (1971).
39. H. Isambert *et al.*, Flexibility of actin filaments derived from thermal fluctuations. Effect of bound nucleotide, phalloidin, and muscle regulatory proteins. *J. Biol. Chem.* **270**, 11437–11444 (1995).
40. R. B. Case, D. W. Pierce, N. Hom-Booher, C. L. Hart, R. D. Vale, The directional preference of kinesin motors is specified by an element outside of the motor catalytic domain. *Cell* **90**, 959–966 (1997).
41. S. Nag *et al.*, Ca2+ binding by domain 2 plays a critical role in the activation and stabilization of gelsolin. *Proc. Natl. Acad. Sci. U.S.A.* **106**, 13713–13718 (2009).
42. J. Schindelin *et al.*, Fiji: An open-source platform for biological-image analysis. *Nat. Methods* **9**, 676–682 (2012).
43. D. Sage, D. Prodanov, J.-Y. Tinevez, J. Schindelin, MIJ: Making interoperablility between ImageJ and Matlab possible. bigwww.epfl.ch/publications/sage1205.html. Accessed ■■■.
44. K. V. Mardia, P. E. Jupp, *Statistics of Directional Data* (John Wiley & Sons, Ltd., Chichester, UK, ed. 2, 2000).
45. Z. Püspöki, M. Storath, D. Sage, M. Unser, Transforms and operators for directional bioimage analysis: A survey. *Adv. Anat. Embryol. Cell Biol.* **219**, 69–93 (2016).
46. R. Rezakhaniha *et al.*, Experimental investigation of collagen waviness and orientation in the arterial adventitia using confocal laser scanning microscopy. *Biomech. Model. Mechanobiol.* **11**, 461–473 (2012).